Optimizing site locations for determining shape from photometric light curves

Daniel O. Fulcoly, Katharine I. Kalamaroff, Francis K. Chun
Department of Physics, U.S. Air Force Academy

ABSTRACT

As satellites become smaller or too far away to visually resolve their physical details via high-resolution imagery, other techniques must be used to characterize and describe them. One promising method is analyzing how the reflected light from a satellite varies as a function of time or phase angle. By analyzing the photometric intensity of the reflected light versus the solar phase angle of the space object, we hope to see a characteristic distribution that is indicative of a certain shape. One way to enhance the analysis is to obtain as many observations of a satellite either through multiple passes over time or by observing a particular satellite pass from numerous locations. This paper is a case study limited to the following question: "Given a certain scenario (orbit, engagement, shape, material, attitude, etc.) and a central sensor location, what is the optimal arrangement of four deployable telescopes for determining the shape of the satellite from its photometric signature?" Certain shapes have a characteristic magnitude-phase angle distribution, especially in its lower boundary which is independent of satellite material and driven primarily by diffusive reflection. The optimum arrangement will be determined by how much of the phase angle coverage is met to determine the lower boundary of the magnitude-phase angle distribution. We will discretize the area surrounding the central site and examine how much of the data is required to determine the satellite shape. Some constraints might be required, such as keeping one telescope in each quadrant or requiring there be a certain distance between sensor sites, to ensure that the optimal arrangement is not a trivial one (i.e. four telescopes at the same location).

1. INTRODUCTION

Space situational awareness (SSA) is the requisite current and predictive knowledge of the space environment and the operational environment upon which space operations depend – including physical, virtual, and human domains – as well as all factors, activities, and events of friendly and adversary space forces across the spectrum of conflict (Codified definition in Joint Pub 3-14, Space Operations). Thus it is helpful to be able to track earth-bound satellites in order to know and predict their position, movement, size, and physical features. However, there are many satellites in orbit that are simply too small or too far away to resolve by conventional optical imaging. Fig. 1 shows the degradation of image quality with increasing distance and decreasing satellite size. By analyzing a satellite's photometric light curve, we hope to obtain some of the same information that one can obtain from high-resolution images.

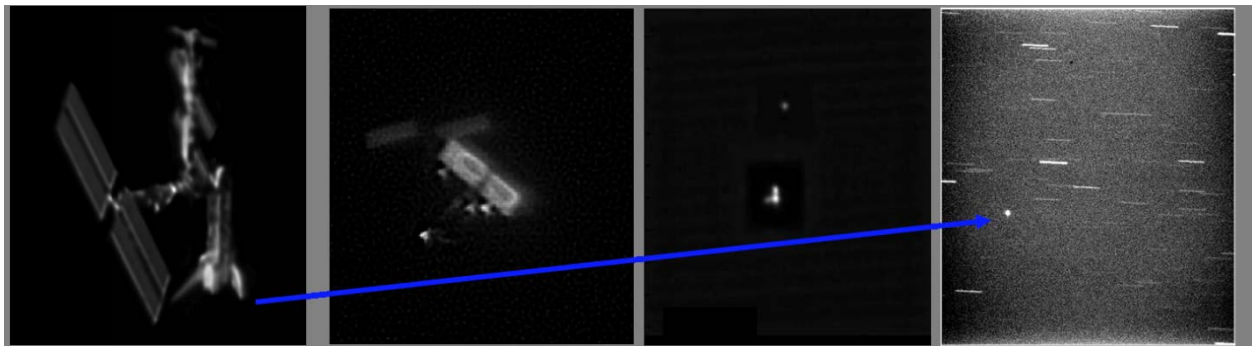

Fig. 1. Degradation of high-resolution images with increasing distance and/or decreasing satellite size.

Report Documentation Page

Form Approved
OMB No. 0704-0188

1. REPORT DATE	2. REPORT TYPE	3. DATES COVERED
SEP 2009		**00-00-2009 to 00-00-2009**

4. TITLE AND SUBTITLE	5a. CONTRACT NUMBER
Optimizing site locations for determining shape from photometric light curves	5b. GRANT NUMBER
	5c. PROGRAM ELEMENT NUMBER
6. AUTHOR(S)	5d. PROJECT NUMBER
	5e. TASK NUMBER
	5f. WORK UNIT NUMBER
7. PERFORMING ORGANIZATION NAME(S) AND ADDRESS(ES) **U.S. Air Force Academy,Department of Physics,USAF Academy ,CO,80840**	8. PERFORMING ORGANIZATION REPORT NUMBER
9. SPONSORING/MONITORING AGENCY NAME(S) AND ADDRESS(ES)	10. SPONSOR/MONITOR'S ACRONYM(S)
	11. SPONSOR/MONITOR'S REPORT NUMBER(S)

12. DISTRIBUTION/AVAILABILITY STATEMENT
Approved for public release; distribution unlimited

13. SUPPLEMENTARY NOTES
2009 Advanced Maui Optical and Space Surveillance Technologies Conference, 1-4 Sep, Maui, HI.

14. ABSTRACT

15. SUBJECT TERMS

16. SECURITY CLASSIFICATION OF:			17. LIMITATION OF ABSTRACT	18. NUMBER OF PAGES	19a. NAME OF RESPONSIBLE PERSON
a. REPORT **unclassified**	b. ABSTRACT **unclassified**	c. THIS PAGE **unclassified**	**Same as Report (SAR)**	**11**	

Light curves are created by measuring the intensity of reflected sunlight off of the object as it passes overhead. The intensity is dependent on a variety of factors to include the size, shape, orientation, and material composition of the satellite. When observing a satellite from different sites, the solar phase angle (i.e. the angle between the site, satellite and sun as illustrated in Fig. 2) determine a great deal about the nature of the light curve. We are interested in determining whether or not there is an optimal arrangement of these angles in order to obtain the most information about the satellite in question. Therefore, we will investigate a variety of pass orientations and site locations and compare the resulting light curves.

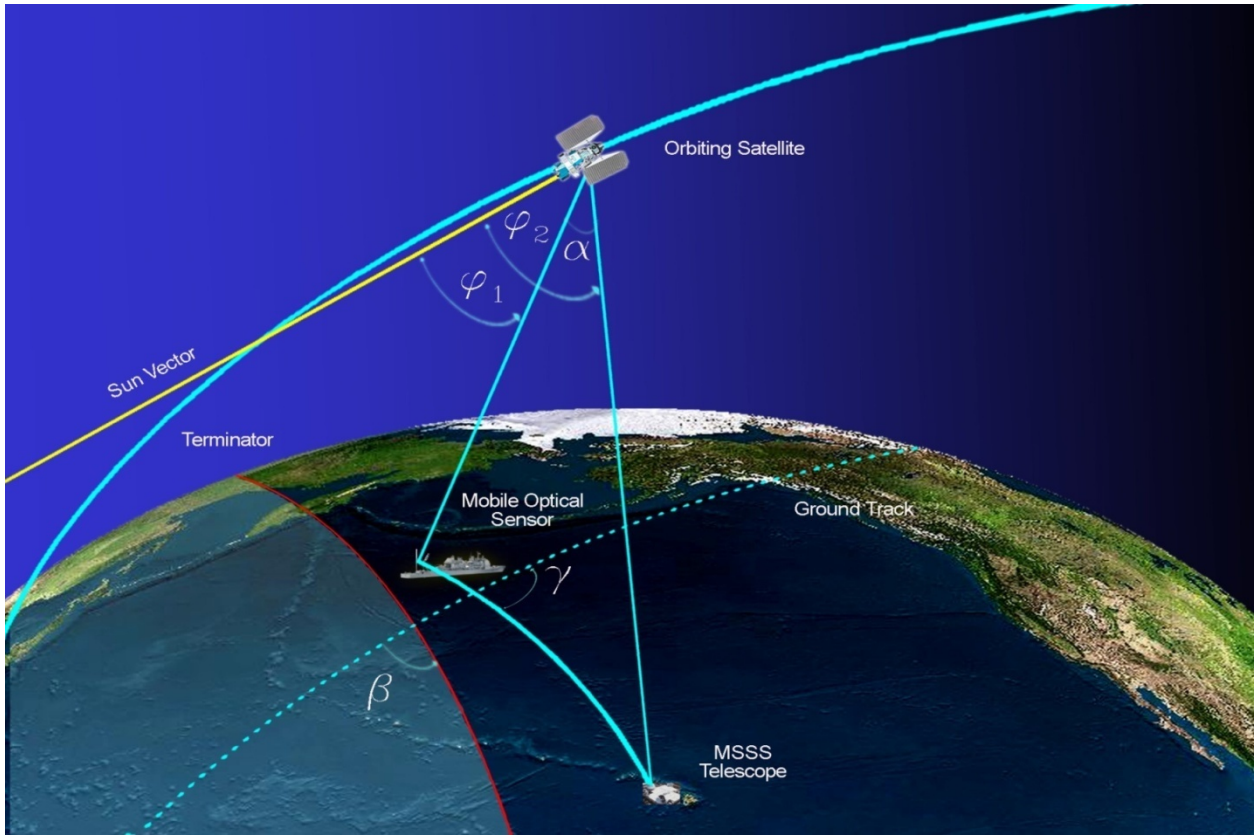

Fig. 2. The photometric light curve of a satellite depends on the geometry of the sensor site, satellite, and sun (drawing courtesy of Betty Duncan, Maui High Performance Computing Center).

2. SIMULATED DATA

All data used in this study was created using a photometric modeling tool developed in MATLAB® by the Directed Energy Directorate of the Air Force Research Laboratory (AFRL). The simulation uses two line elements (TLEs) to determine satellite pass geometry and allows a user to define satellite size, shape, material, and attitude as well as observation location. This tool has been used in the past by AFRL to investigate various non-resolvable space object identification problems such as analyzing when single facets become visible or illuminated by the sun as viewed from closely spaced observers [1]. A version of this tool has also been used to investigate glints from cubesats [2].

The first step to choosing the optimal site locations is to decide on criteria for determining what is optimal, which itself depends on the question one is trying to answer. For this study, an optimal combination of sites would be one

that can determine the satellite's shape with the highest certainty. We used a version of the photometric modeling tool that created Monte Carlo scans of different shapes compiled into intensity versus solar phase angle distributions as our analysis "standard". These distributions are influenced by a satellite's shape, size, and material. As seen in Fig. 3, each shape has a unique lower bound (or minimum intensity envelope) and, in particular, an asymptotic cutoff angle. It is thought that the lower bound curve is governed by a satellite's diffuse reflection whereas the rest of the distribution is a combination of both its diffuse and specular reflection [1]. For instance, for a cube-shaped satellite (top middle panel), the minimum intensity has a cutoff solar phase angle of 90°, which corresponds to a facet normal visible to an observer being 90° to the sun. For a tetrahedron, the cutoff solar phase angle is 54.7° ( ) corresponding to the angle between a face and an edge [3]. The relative position of the distribution along the intensity axis is indicative of the material and size of a satellite, and is not related to its shape.

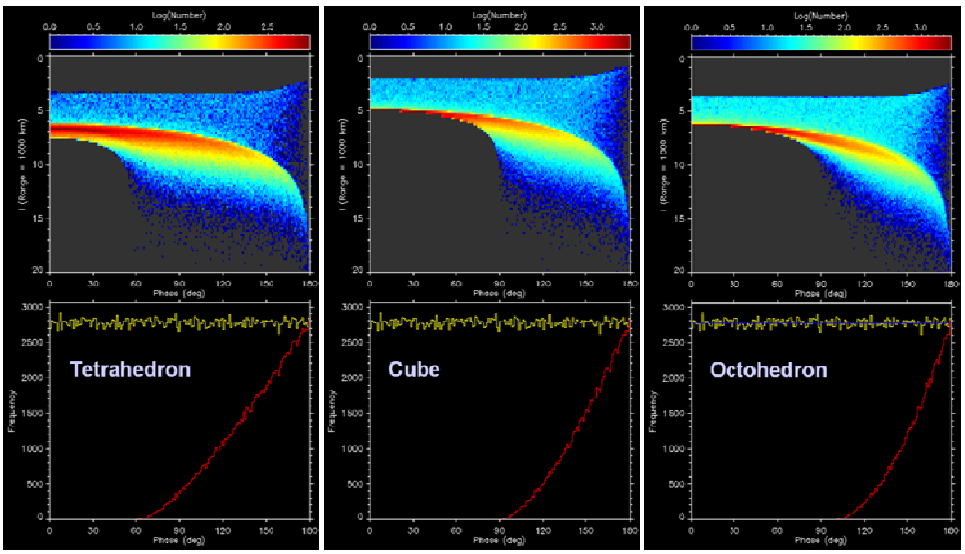

Fig. 3. The top graphs (color plots) are distributions of a satellite's reflected intensities (*y*-axis) with respect to phase angle (*x*-axis) at varying attitudes. The yellow line in the bottom graphs are histograms of the number of observations with respect to phase angle. The red line in the bottom curve is a histogram of the number of observations with no reflected light with respect to phase angle (Figures courtesy of Dr. Doyle Hall (Boeing) and Mr. Paul Kervin (AFRL) and similar to those in Reference [1])

Rather than compare our sample data to the entire distributions, we only used the lower bound curves of the Monte Carlo distributions. These curves were extracted from the graphs in Fig. 3 above by binning the distributions in one-degree solar phase angle intervals and selecting the minimum intensity data point in each bin. The first points of each curve were then normalized to the same value to account for differences in material. Three shapes were initially chosen for this case study, a tetrahedron, cube, and octahedron. Their lower bound curves derived from the Monte Carlo scans are shown in Fig. 4. Based on the extreme similarity between the cube and the octahedron, the octahedron was set aside until an algorithm was devised that could distinguish between a cube and a tetrahedron. The lower bound curves and respective cutoff angles were then compared to a sample set of simulated photometric data as described in the next section.

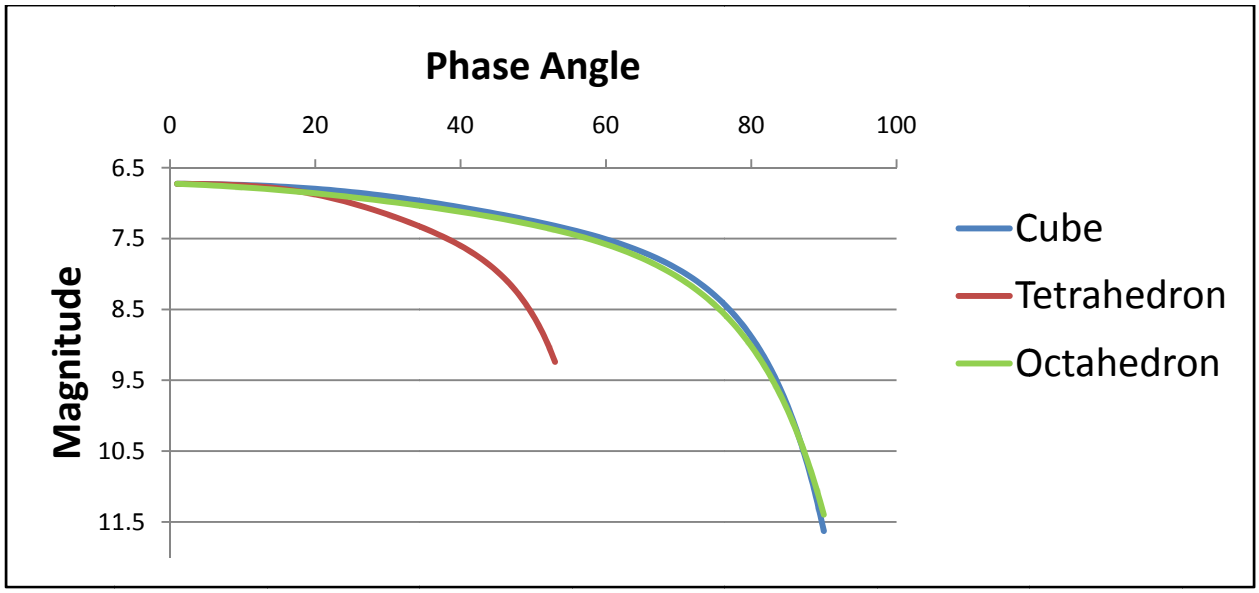

Fig. 4. Lower bound curves for three chosen shapes.

2.1. Multiple Sensor Sites

Fig. 5 shows a sample orbit for SSN 13736 (DMSP F6) which has an altitude of 820 kilometers, an inclination of 98.62º, a right ascension of 55.78º, and an eccentricity of 0.0008. The sensor site location chosen is the Advanced Electro-Optical Site (AEOS) on Haleakala, Maui, Hawaii. We define the multi-site domain as a circular region centered on the central sensor location divided into four quadrants akin to Cartesian coordinates. The sites are identified by their radius and angle (clockwise from North) as illustrated in Fig. 5.

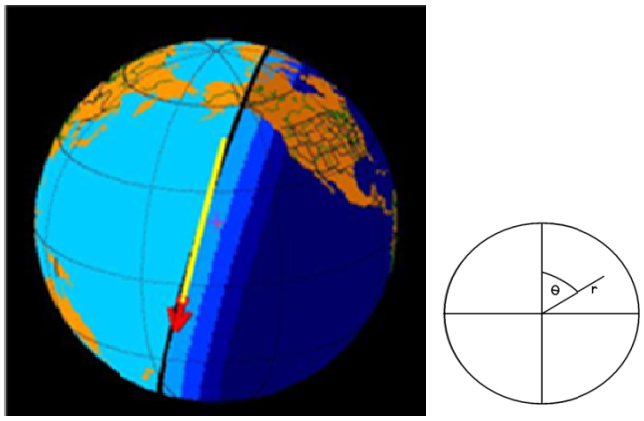

Fig. 5. Sample satellite pass (left) and the multi-site definition (right).

The spatial resolution of the multi-site domain is 1 degree and 10 radii levels, with each radius representing 111 kilometers or a single degree of latitude and longitude, giving the domain a total diameter of 2,220 kilometers and 3,600 sites. We modified the AFRL photometric tool to run in a parallel processing environment, creating two parallel versions, one that would take a single sensor site and process the number of possible passes of a specified satellite throughout a specified time period such as a year [4]. The second version was used for this study and allowed us to process 3,600 sensor sites for a given satellite pass on a specified date and time period. Fig. 6 shows the basic flow of the parallel site version.

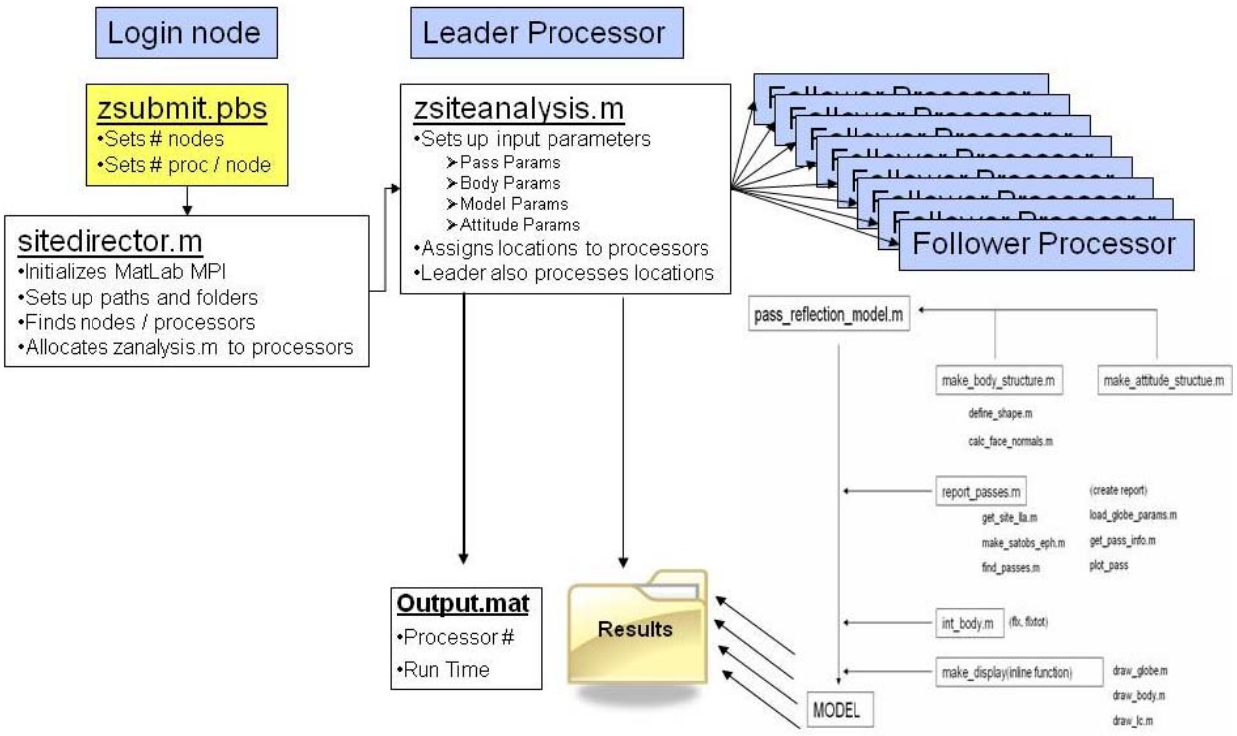

Fig. 6. Flow chart of the parallel version of the multi-site photometric modeling tool.

An example of the data from all the sensor sites can be seen in Fig. 7 below. On the left is the ground track of the satellite along with all 3,600 sensor locations. The central location (AEOS) is indicated by the crossed circle in the center. The dark blue regions to the far right of the ground track indicate sensor sites which could not see the satellite and thus had no photometric light curve. The lighter blue region surrounding the ground track indicate that the sensor sites saw a similar light curve as AEOS. As one then moves to the left, the sensor sites see increasingly different light curves than AEOS. Six representative sensor sites are chosen to illustrate the difference in the light curves. The corresponding magnitude-phase angle distribution for the six sites along with the AEOS site are shown in the graph to the right.

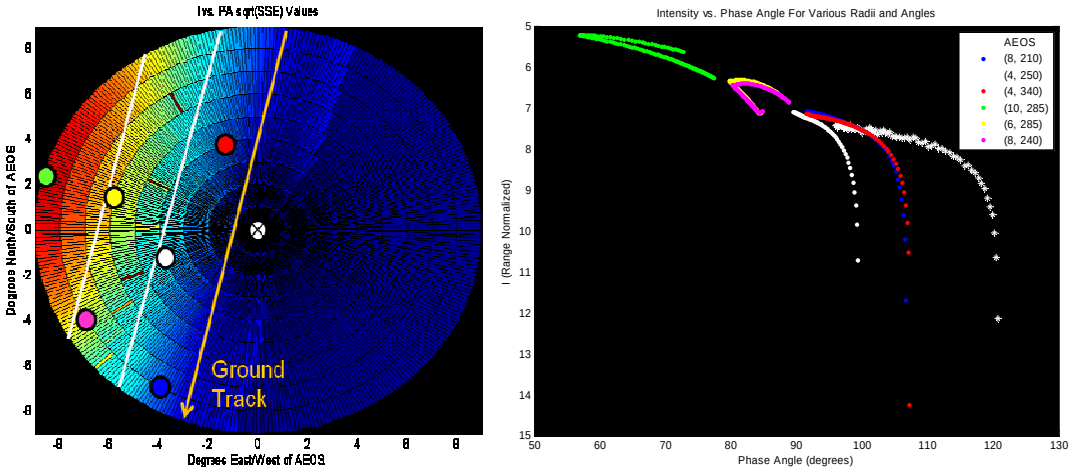

Fig. 7. Example of 3,600 sensor sites centered along AEOS for a satellite track. The colored circles on the left plot corresponds to the colored lines in the magnitude-phase angle plot of the right. The AEOS magnitude-phase-angle distribution is the white crossed data points on the far right of the right plot.

Since each quadrant contains 900 sites, there are 656 billion possible site combinations. Analysis of all possible site combinations would ultimately require high performance computing. Thus we initially limited the number of combinations so that a viable shape-determination algorithm could be developed serially. Once an algorithm shows promise, it can be applied to all possible site combinations. The combination that returns the highest certainty (along with the correct answer) would become the optimum site combination. Different pass geometries will most likely yield different optimal combinations, and eventually one could combine this data into an optimal combination for any geometry.

To compile a sample data set, we combined data from one satellite pass observed from four different sensor locations each which had approximately 50-100 data points for a total sample data set size of 200-400 points. However, since we only needed a lower bound curve from the sample data, we had to decimate the sample set. This was done in three steps and is illustrated in Fig. 8. The first step was to bin the data into one degree phase angle intervals and keep the lowest intensity data point. While all of the points remaining at this point are technically on the sample set minimum curve, they might stand out as not being real candidates for an actual lower bound curve. Thus for the second step, we removed any point which was brighter (i.e. smaller magnitude) than the point to the left of it (at a smaller phase angle). The final step was based on the fact that lower bound curves are similar to increasing/decreasing functions meaning that the concavity of its shape should not change. Accordingly, we calculated a slope between all neighboring points. If a slope was less steep than the preceding slope, the trailing point was discarded. Fig. 8 below shows how a sample data set evolves into a lower bound curve based on the above three steps.

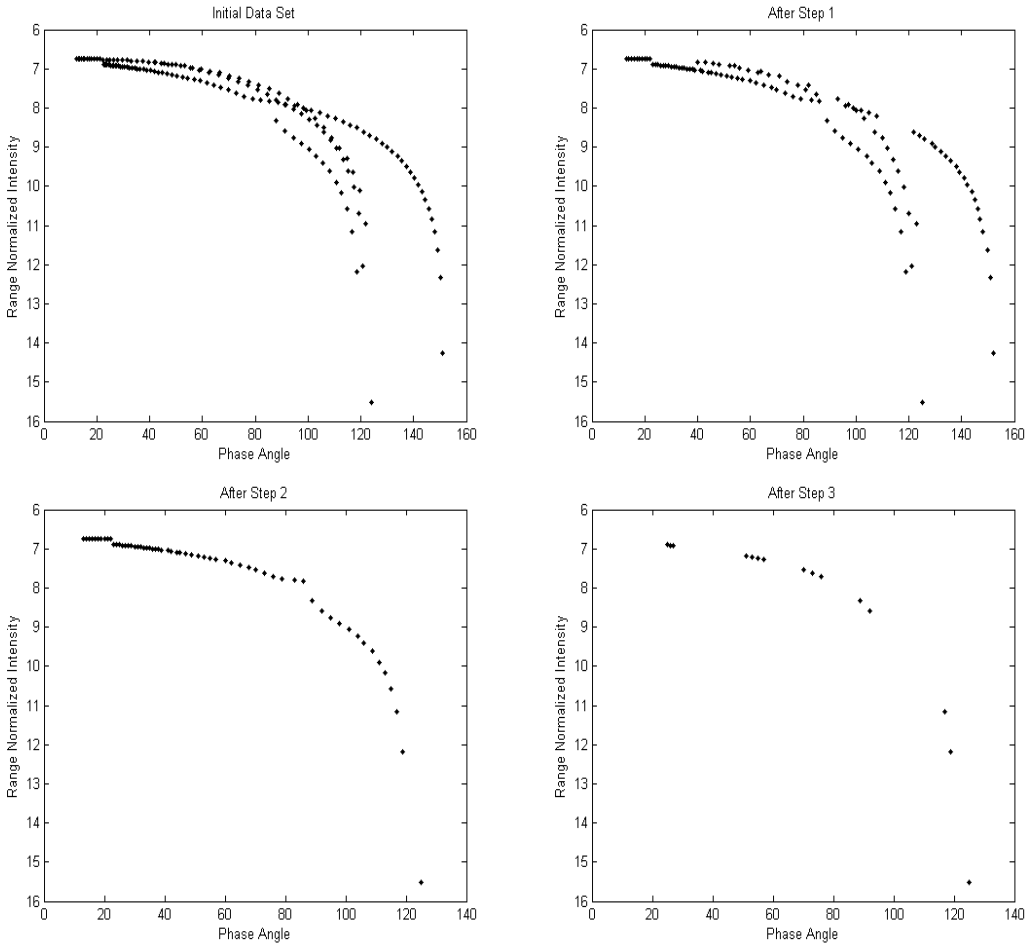

Fig. 8. An initial data set is trimmed to exclude points not likely to be on the lower bound curve.

Now that the sample sets and comparison sets have been built, the question remains as to how to compare them. Three methods were explored in this study, mean squared error (MSE), curve fitting, and analysis of variance (ANOVA) of residuals. These methods are discussed in the next section except for the ANOVA method as it was quickly discovered to be completely unreliable.

2.2. Mean Squared Error

The mean squared error was found by calculating the difference between each sample set data point and the intensity value from the known lower bound curves corresponding to the phase angle bin. The sample data set was shifted so that the first sample point had zero difference since we want to negate material or size differences. The mean squared error was then calculated for each shape, and the shape with the lowest MSE was the determined shape. Eq. (1) shows how MSE was calculated.

$$MSE_{shape} = \frac{\sum_{\phi}^{n} \left[\left(Intensity(\phi)_{shape} - Offset_{shape} \right) - SampleIntensity(\phi) \right]^2}{\#\,Observations} \tag{1}$$

2.3. Curve Fitting

This method stemmed from the observation that lower bound curves seem to behave like exponential functions. Data sets were trimmed such that they had no points with phase angles greater than the hypothesized cutoff angle, ϕ_c (55° for tetrahedron and 90° for cube), and then fit with a non-linear least squares (trust region) scheme. The functional form, shown in Eq. (2), was chosen because of its asymptotic behavior. All constants were constrained to be positive to keep the asymptote in the correct direction.

$$f(\phi) = a + \frac{b}{(\phi - \phi_c)^2} + \frac{c}{(\phi - \phi_c)^4} + \frac{d}{(\phi - \phi_c)^6} + \frac{e}{(\phi - \phi_c)^8} \tag{2}$$

The shape whose fit had the lowest reduced chi-squared value (χ_r^2) was the answer returned by the algorithm. One advantage of this method was that it gave a metric (χ_r^2) for comparing the certainty of different combinations.

3. EXPERIMENTAL RESULTS

For the purpose of testing different shape-determination algorithms, we took a subset of all possible 3,600 sensor locations, using 3 radii and 3 angles per quadrant for a total of 6,561 combinations. Each test case was a specific shape (tetrahedron or cube) and satellite pass. Table 1 below lists the four satellite element sets used in this study and the six time periods in which we determined passes of various orientations to the terminator. Thus there was a total of 12 test cases. All test cases had the same bidirectional reflectance distribution (BRDF), a Cook-Torrance BRDF of 30% diffusive and 30% specular reflectance. Additionally, the satellite attitudes were the same fixed ram-nadir orientation with the body *x*-axis pointing to the ram direction and the body *z*-axis pointing to nadir. Finally, all the simulated objects had a size perfectly inscribable into a one meter diameter sphere

Table 1. Satellite passes used to create multiple site locations.

SSN (Common Name)	Date	Start UT	End UT
13736 (DMSP 5D-2 F6)	January 1, 2007	05:00:00	06:00:00
28773 (ASTRO E2)	January 5, 2007	15:15:00	16:15:00
28773 (ASTRO E2)	February 5, 2007	04:15:00	05:15:00
25544 (ISS)	February 12, 2007	04:15:00	05:15:00
28773 (ASTRO E2)	June 26, 2007	07:15:00	08:15:00
30776 (FALCONSAT 3)	January 1, 2008	15:15:00	16:15:00

The results for the MSE method were unimpressive. When applied to the 12 test cases, this method gave the correct answer 6 times. All six of these cases were cubes however, and all tetrahedron cases failed. The total success rate was 53%, with the cube success rate at 100% and the tetrahedron success rate at 5%. The algorithm had a tendency to return an answer of cube, and an examination of our sample data showed why. The lower bound curves for our sparser four-site data set did not match those of the Monte Carlo scans. This could be due to the stabilized attitude of the simulated satellites and possibly to the limited number of satellite pass orientations used in this study.

For the curve fitting algorithm method, 7 of the 11 cases (one case failed) resulted in a correct answer. The total success rate was once again 53%, with the cube success rate at 37% and the tetrahedron success rate at 71%. Fig. 9 shows the results for the curve fitting method on a case by case basis. Fig. 10 is a specific example for the curve fitting method for Case 6 (SSN 28773, January 5, 2007) for a tetrahedron object. Although this example converged to the correct shape nearly 100% of the time, one can see that when compared to the actual data (black line), to first order the cube fit (green line) appears to match the data better than the tetrahedron fit (red line). However, the χ_r^2 for the tetrahedron fit and data was better than the one for the cube fit and data.

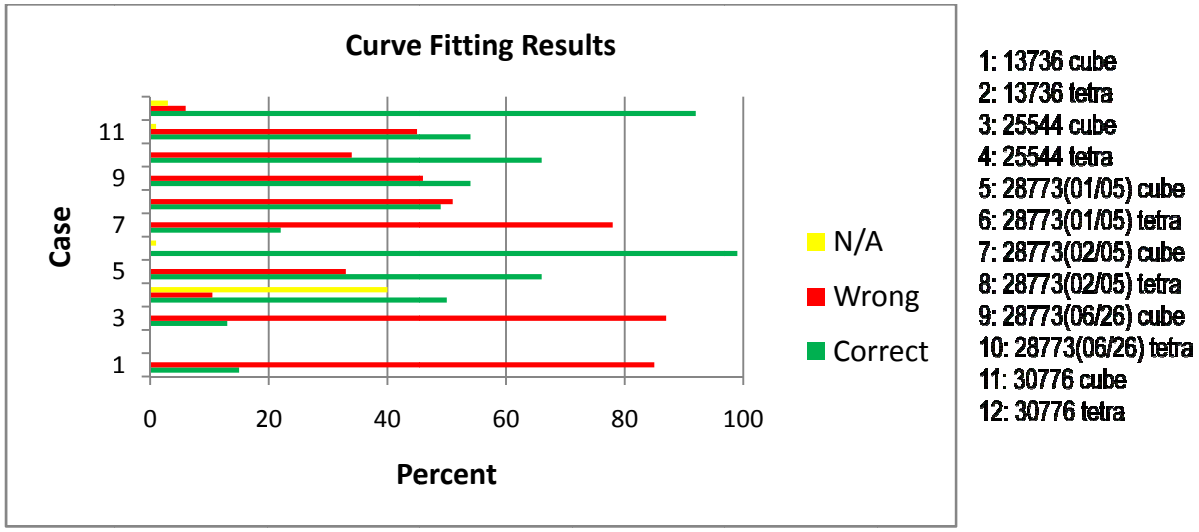

Fig. 9. The experimental results for the curve fitting algorithm. The numbered cases are listed at right.

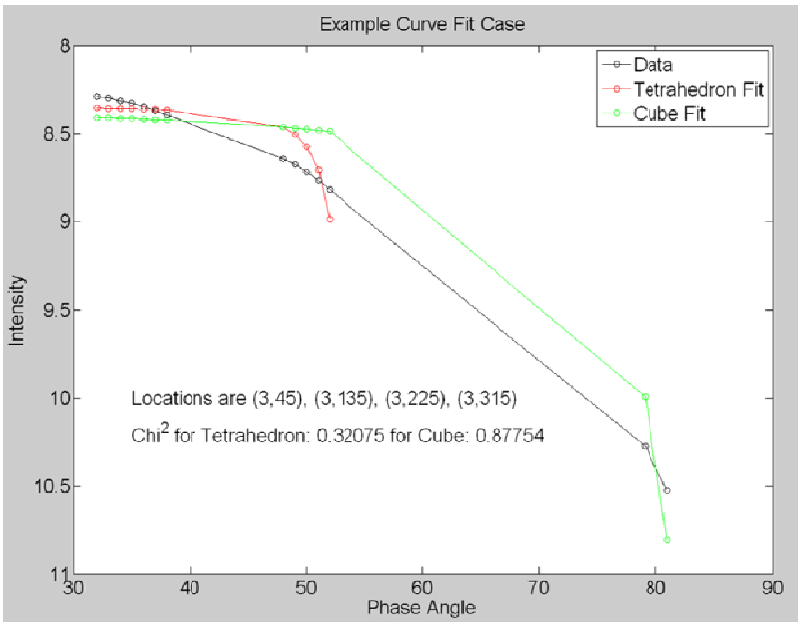

Fig. 10. One example used in the curve fitting algorithm for SSN 28773, January 1, 2007 (tetrahedron).

4. DISCUSSION

The relative failure of both these methods seems somewhat suspect based on the clear difference in lower bound curves for tetrahedrons and cubes. A closer investigation, as shown in Fig. 11, reveals that the lower bound curves for our simulated data does not bear a striking resemblance to the Monte Carlo scans shown earlier (Fig. 3). While the cube data (left plot) appears to initially follow the lower bound curve seen in the Monte Carlo scans, between 80° and 120° of phase angle there are no low intensity points to demonstrate an asymptotic relationship. The same observation holds for the tetrahedron data (right plot); there are no low intensity data points until nearly 30° of phase angle past the predicted 54.7° phase angle cutoff. How can we compare to asymptotic curves if our simulated data doesn't show the same pattern? The pattern below most likely lies in that the simulated satellites all had stabilized attitude, specifically nadir and ram pointing. The Monte Carlo scans were created by simulating the shape in hundreds of different orientations for each phase angle. Since the same face is observed nearly constantly for each pass, we are not seeing the orientations that drive the asymptotic lower bound curves. Only in very rare cases will either of these methods be viable in determining the shape of a stable satellite.

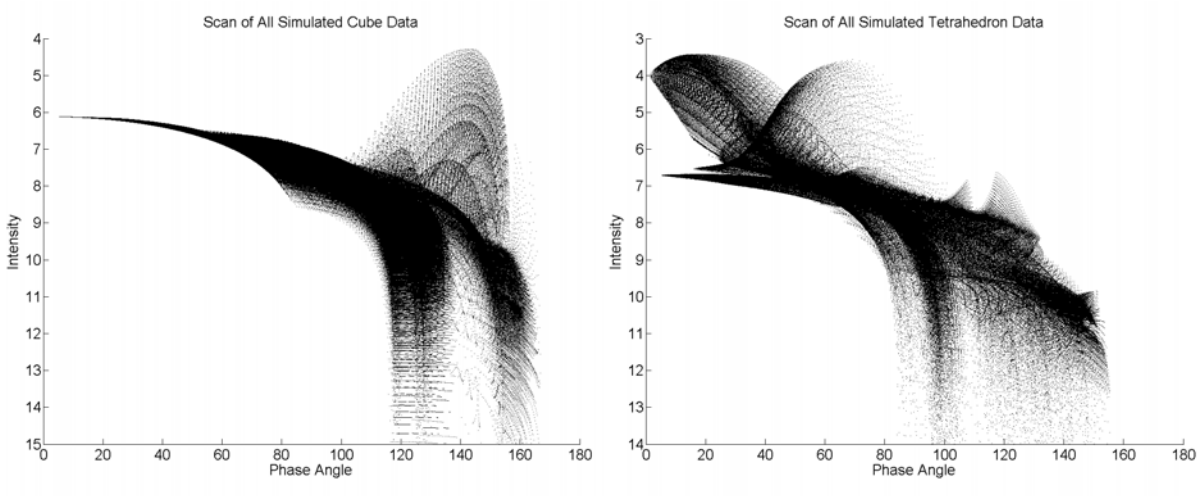

Fig. 11. Distribution of all simulated cube (left panel) and tetrahedron (right panel) data for the 12 test cases.

5. CONCLUSIONS

The two methods attempted, mean squared error and curve fitting, both failed to convincingly identify satellite shape using simulated data from combinations of four sensor sites. Although the MSE method selected the cube 100% of the time, its correctness could be attributed to a bias toward selecting the cube. The curve fitting method appears to correctly choose the tetrahedron more often than not, but more work needs to be done in order to quantify the confidence in this method (especially for other shapes). The main issue however, could be the fact that we are making an erroneous comparison. The Monte Carlo scans are based on hundreds of attitudes for any given phase angle, whereas our simulated sensor site data contained a very small range of attitudes due to the stability of the simulated satellites. The question of optimal site locations cannot be definitively answered due to the inability of either algorithm to succeed at shape determination. Currently, we are working to incorporate simulated data for a spinning object using the same shapes and satellite passes in order to see if the data is more similar to the Monte Carlo scans.

6. ACKNOWLEDGEMENTS

The authors would like to thank Dr. Doyle Hall and Mr. Paul Kervin for the use of their photometric modeling tool, their insight as to how to interpret the lower bound curves for different shapes, and their overall comments, suggestions, and recommendations. We also thank the Department of Defense High Performance Computing Modernization Program Office, the Maui High Performance Computing Center and Detachment 15, Air Force Research Laboratory for their support to the U.S. Air Force Academy Cadet Summer Research Program under which much of this research was conducted. Finally, this research was funded in part by Dr. Kent Miller of the Air Force Office of Scientific Research and Mr. Joe Koesters of the Sensors Directorate, Air Force Research Laboratory.

7. REFERENCES

1. Hall D. et. al., “Separating Attitude and Shape Effects for Non-resolved Objects,” *The 2007 AMOS Technical Conference Proceedings*, Kihei, HI, 2007.

2. Hall D., “Optical CubeSat Discrimination,” *The 2008 AMOS Technical Conference Proceedings*, Kihei, HI, 2007.

3. "Tetrahedron." *Wikipedia, The Free Encyclopedia*. 17 Aug 2009, 18:23 UTC. 17 Aug 2009 <http://en.wikipedia.org/w/index.php?title=Tetrahedron&oldid=308522581>.

4. Kalamaroff K. and Chun F., "Simulation of Space Object Time-Resolved Signatures," *Maui High Performance Computing Center Application Briefs*, 2009.